Fiber optic microendoscopy for preclinical study of bacterial infection dynamics

Nooman Mufti,[1,3] Ying Kong,[2,3] Jeffrey D. Cirillo,[2] and Kristen C. Maitland[1,*]

[1]*Department of Biomedical Engineering, Texas A&M University, 337 Zachry Engineering Center, 3120 TAMU, College Station, TX 77843, USA*

[2]*Department of Microbial and Molecular Pathogenesis, Texas A&M Health Science Center, 467 Reynolds Medical Building, College Station, TX, 77843, USA*

[3]*These authors contributed equally to this work*

**kmaitland@tamu.edu*

Abstract: We explore the use of fiber optic microendoscopy to image and quantify bacterial infection in the skin and lungs using an animal model. The contact probe fiber bundle fluorescence microendoscope has a 4 μm resolution, a 750 μm field of view, and a 1 mm outer diameter. Subcutaneous and intra-tracheal infections of fluorescent *Mycobacterium bovis* Bacillus Calmette-Guérin (BCG) bacteria were detected *in situ* from inocula down to 10^4 and 10^7 colony forming units, respectively.

OCIS codes: (170.2150) Endoscopic imaging; (170.3880) Medical and biological imaging; (110.0110) Imaging systems; (060.2350) Fiber optics imaging.

References and links

1. Centers for Disease Control, "Tuberculosis (TB): Data and Statistics," Oct. 25, 2010, retrieved Feb. 16, 2010, http://www.cdc.gov/tb/statistics/default.htm.
2. M. Taniguchi, E. Akai, T. Koshida, K. Hibi, H. Kudo, K. Otsuka, H. Saito, K. Yano, H. Endo, and K. Mitsubayashi, "A fiber optic immunosensor for rapid bacteria determination," in *3rd Kuala Lumpur International Conference on Biomedical Engineering 2006*, F. Ibrahim, N. A. Abu Osman, J. Usman, and N. A. Kadri, eds. (Springer-Verlag, Berlin, 2007), pp. 308–311.
3. M. S. John, A. Kishen, L. C. Sing, and A. Asundi, "Determination of bacterial activity by use of an evanescent-wave fiber-optic sensor," Appl. Opt. **41**(34), 7334–7338 (2002).
4. H. E. Giana, L. Silveira, Jr., R. A. Zangaro, and M. T. T. Pacheco, "Rapid identification of bacterial species by fluorescence spectroscopy and classification through principal components analysis," J. Fluoresc. **13**(6), 489–493 (2003).
5. C. H. Contag, P. R. Contag, J. I. Mullins, S. D. Spilman, D. K. Stevenson, and D. A. Benaron, "Photonic detection of bacterial pathogens in living hosts," Mol. Microbiol. **18**(4), 593–603 (1995).
6. J. Sjollema, P. K. Sharma, R. J. B. Dijkstra, G. M. van Dam, H. C. van der Mei, A. F. Engelsman, and H. J. Busscher, "The potential for bio-optical imaging of biomaterial-associated infection in vivo," Biomaterials **31**(8), 1984–1995 (2010).
7. S. Wiles, K. M. Pickard, K. Peng, T. T. MacDonald, and G. Frankel, "In vivo bioluminescence imaging of the murine pathogen Citrobacter rodentium," Infect. Immun. **74**(9), 5391–5396 (2006).
8. N. A. Kuklin, G. D. Pancari, T. W. Tobery, L. Cope, J. Jackson, C. Gill, K. Overbye, K. P. Francis, J. Yu, D. Montgomery, A. S. Anderson, W. McClements, and K. U. Jansen, "Real-time monitoring of bacterial infection in vivo: development of bioluminescent staphylococcal foreign-body and deep-thigh-wound mouse infection models," Antimicrob. Agents Chemother. **47**(9), 2740–2748 (2003).
9. Y. Kong, S. Subbian, S. L. G. Cirillo, and J. D. Cirillo, "Application of optical imaging to study of extrapulmonary spread by tuberculosis," Tuberculosis (Edinb.) **89**(Suppl 1), S15–S17 (2009).
10. V. Balasubramanian, E. H. Wiegeshaus, B. T. Taylor, and D. W. Smith, "Pathogenesis of tuberculosis: pathway to apical localization," Tuber. Lung Dis. **75**(3), 168–178 (1994).
11. A. F. Gmitro and D. Aziz, "Confocal microscopy through a fiber-optic imaging bundle," Opt. Lett. **18**(8), 565–567 (1993).
12. J. Knittel, L. Schnieder, G. Buess, B. Messerschmidt, and T. Possner, "Endoscope-compatible confocal microscope using a gradient index-lens system," Opt. Commun. **188**(5-6), 267–273 (2001).
13. K.-B. Sung, C. Liang, M. Descour, T. Collier, M. Follen, and R. Richards-Kortum, "Fiber-optic confocal reflectance microscope with miniature objective for in vivo imaging of human tissues," IEEE Trans. Biomed. Eng. **49**(10), 1168–1172 (2002).
14. K. Carlson, M. Chidley, K. B. Sung, M. Descour, A. Gillenwater, M. Follen, and R. Richards-Kortum, "In vivo fiber-optic confocal reflectance microscope with an injection-molded plastic miniature objective lens," Appl. Opt. **44**(10), 1792–1797 (2005).

#142906 - $15.00 USD Received 23 Feb 2011; revised 2 Apr 2011; accepted 4 Apr 2011; published 7 Apr 2011

15. A. R. Rouse, A. Kano, J. A. Udovich, S. M. Kroto, and A. F. Gmitro, "Design and demonstration of a miniature catheter for a confocal microendoscope," Appl. Opt. **43**(31), 5763–5771 (2004).
16. T. J. Muldoon, M. C. Pierce, D. L. Nida, M. D. Williams, A. Gillenwater, and R. Richards-Kortum, "Subcellular-resolution molecular imaging within living tissue by fiber microendoscopy," Opt. Express **15**(25), 16413–16423 (2007).
17. J. Sun, C. Shu, B. Appiah, and R. Drezek, "Needle-compatible single fiber bundle image guide reflectance endoscope," J. Biomed. Opt. **15**(4), 040502 (2010).
18. T. J. Muldoon, S. Anandasabapathy, D. Maru, and R. Richards-Kortum, "High-resolution imaging in Barrett's esophagus: a novel, low-cost endoscopic microscope," Gastrointest. Endosc. **68**(4), 737–744 (2008).
19. W. Zhong, J. P. Celli, I. Rizvi, Z. Mai, B. Q. Spring, S. H. Yun, and T. Hasan, "In vivo high-resolution fluorescence microendoscopy for ovarian cancer detection and treatment monitoring," Br. J. Cancer **101**(12), 2015–2022 (2009).
20. M. Hirano, Y. Yamashita, and A. Miyakawa, "In vivo visualization of hippocampal cells and dynamics of Ca2+ concentration during anoxia: feasibility of a fiber-optic plate microscope system for in vivo experiments," Brain Res. **732**(1-2), 61–68 (1996).
21. S. Gordon, S. Keshav, and M. Stein, "BCG-induced granuloma formation in murine tissues," Immunobiology **191**(4-5), 369–377 (1994).
22. M. Goldgeier, C. A. Fox, J. M. Zavislan, D. Harris, and S. Gonzalez, "Noninvasive imaging, treatment, and microscopic confirmation of clearance of basal cell carcinoma," Dermatol. Surg. **29**(3), 205–210 (2003).
23. N. C. Shaner, P. A. Steinbach, and R. Y. Tsien, "A guide to choosing fluorescent proteins," Nat. Methods **2**(12), 905–909 (2005).
24. N. C. Deliolanis, R. Kasmieh, T. Wurdinger, B. A. Tannous, K. Shah, and V. Ntziachristos, "Performance of the red-shifted fluorescent proteins in deep-tissue molecular imaging applications," J. Biomed. Opt. **13**(4), 044008 (2008).
25. A. Mohan and S. K. Sharma, "Fibreoptic bronchoscopy in the diagnosis of sputum smear-negative pulmonary tuberculosis: current status," Indian J. Chest Dis. Allied Sci. **50**(1), 67–78 (2008).
26. K. C. Ganguly, M. M. Hiron, Z. U. Mridha, M. Biswas, M. K. Hassan, S. C. Saha, and M. M. Rahman, "Comparison of sputum induction with broncho-alveolar lavage in the diagnosis of smear-negative pulmonary tuberculosis," Mymensingh Med. J. **17**(2), 115–123 (2008).
27. Y. Kong, H. Yao, H. Ren, S. Subbian, S. L. Cirillo, J. C. Sacchettini, J. Rao, and J. D. Cirillo, "Imaging tuberculosis with endogenous beta-lactamase reporter enzyme fluorescence in live mice," Proc. Natl. Acad. Sci. U.S.A. **107**(27), 12239–12244 (2010).

1. Introduction

Bacterial infections, including tuberculosis, affect a large segment of the world's population. Centers for Disease Control estimates indicate one-third of the world's population is currently infected with tuberculosis [1]. The disease has an incubation period that varies from a few weeks to years, thereby complicating early stage diagnosis and necessitating a cocktail of antibiotics for treatment once it is diagnosed. Study of early stage bacterial pathogenesis, particularly in the case of tuberculosis, is imperative to the design of better clinical diagnostic and therapeutic techniques to help combat this disease.

Researchers have developed optical biosensors that can detect bacteria in various *ex vivo* samples [2–4]. Whole body fluorescence imaging scanners [5,6] are also being developed for non-invasive, *in vivo* detection and real-time monitoring of growth using bioluminescent and fluorescent versions of bacteria such as *Citrobacter rodentium* and *Escherichia coli* [7], *Staphylococcal aureus* [8] and *Mycobacterium bovis* [9] throughout the body in preclinical studies. However, due to the depth of the infected tissue, such as lung tissue in the case of tuberculosis, tissue absorption and scattering of photons emitted by the low numbers of bacteria present precludes the possibility of using these systems for early stage quantification of bacterial infections. Although detection limits for macroscopic imaging systems have been reported down to 10^2 colony forming units (CFU) for *in vitro* samples, 10^5 CFU has been reported as a limit of detection for *in vivo* subcutaneous infections using bioluminescent and fluorescent bacteria [8,9]. Owing to the highly light scattering nature of the lungs, pulmonary infections with intra-tracheal dosage levels greater than 10^5 CFU are typically employed. However, since the infectious dose for tuberculosis is thought to be as low as 1-10 bacteria [10], improving this threshold of detection is a high priority. A system that can image and quantify pulmonary bacterial infection with intra-tracheal inocula below 10^5 CFU during the first few days following infection to model early stage and low bacterial load infections would be very valuable for research on infectious diseases.

#142906 - $15.00 USD Received 23 Feb 2011; revised 2 Apr 2011; accepted 4 Apr 2011; published 7 Apr 2011

Endoscopes that utilize fiber optic elements to relay real-time reflectance or fluorescence signals from tissues and organs *in vivo* are in common use in the healthcare sector. Optical fiber bundles have been exploited in high resolution confocal microendoscopes [11,12] with high numerical aperture miniature objective lenses [13–15]. Simplified contact probe microendoscopes with wide-field illumination have more recently been developed [16,17] and evaluated as tools for cancer detection [18,19] and brain imaging [20]. Although major advances in optical fiber based high resolution *in vivo* imaging systems have been achieved in the field of early cancer detection, to our knowledge, fiber optic microendoscopy has not yet been applied to *in vivo* imaging and detection of bacteria. Such a fiber based fluorescence imaging system is uniquely suited for the detection and imaging of small regions of bacterial infection inside live animals. It can serve as a valuable tool for study of the early stage *in vivo* dynamics of bacterial infection, especially when used with whole body imaging systems.

2. Methods

2.1. Optical system design

Figure 1 illustrates the layout of the fluorescence microendoscope. The basic design is similar to the system developed by Muldoon et al. for early cancer detection in epithelial tissue [16]. Excitation and emission wavelengths were selected for detection of fluorescence from tdTomato. A light emitting diode (LED) source (Luxeon LumiLED) with a 70 nm bandwidth centered at 530 nm is used as an excitation source. The light is collimated by a 10x achromatic doublet objective lens (Leica), filtered by a 40 nm bandwidth excitation filter (Semrock, FF01-531/40) and dichroic mirror (Semrock, FF562-Di), and focused onto a fiber bundle (Sumitomo IGN-08/30) by another 10x objective lens (Leica). The 1 mm outer diameter fiber bundle consists of 30,000 individual fibers. The 4 μm nominal fiber core-to-core spacing determines the system's resolution, and 750 μm active imaging diameter determines the imaging field of view [16]. The fiber bundle transmits the excitation light to its distal tip, which is placed directly in contact with the sample. The resulting fluorescence light from the sample is collected by the same fiber bundle, filtered by a 54 nm bandwidth emission filter (Semrock, FF01-609/54) centered at 609 nm, and imaged onto a scientific grade 1.45 megapixel CCD camera (QImaging Exi Blue) with 6.45 μm x 6.45 μm pixel size. A 150 mm focal length achromatic doublet tube lens (Thorlabs, LSB08-A) and the 10x objective lens provide a magnification of 8.2x to focus the entire active imaging diameter of the fiber bundle onto the 2/3 inch (diagonal) CCD camera.

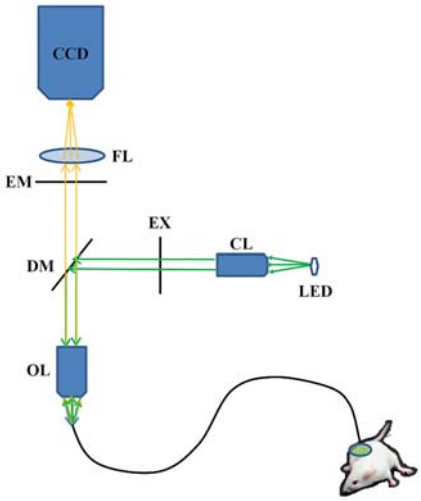

Fig. 1. Schematic of fluorescence microendoscope for preclinical imaging. LED: light emitting diode, CL: collimating lens, EX: excitation filter, DM: dichroic mirror, OL: objective lens, EM: emission filter, FL: focusing lens, CCD: charge coupled device camera.

#142906 - $15.00 USD Received 23 Feb 2011; revised 2 Apr 2011; accepted 4 Apr 2011; published 7 Apr 2011

2.2. In vitro imaging of bacterial colonies

Mycobacterium bovis Bacillus Calmette-Guérin (BCG) bacteria, an attenuated form of the live bovine tuberculosis bacillus, *Mycobacterium bovis* and used as a vaccine for *Mycobacterium tuberculosis*, was used in all the experiments. BCG was chosen for this study for safety considerations owing to their lack of virulence in humans. However, their ability to infect and persist within mammalian tissue is similar to the pathogenic mycobacteria [21]. BCG bacterial colonies expressing the fluorescent protein tdTomato and a negative control of non-fluorescent BCG with vector backbone were grown in colonies on agar. tdTomato was selected as the fluorescent protein because it has a greater quantum yield of 0.69 as compared to 0.6 for common fluorescent proteins such as the enhanced form of GFP (EGFP) [22], as well as a brightness (product of quantum yield and extinction coefficient) that is 2.8 times greater than EGFP [23]. Moreover, being a red-shifted protein, it has the advantage of emitting in the 580-700 nm wavelength range, where there is reduced light absorption due to hemoglobin in tissue [24]. The probe was placed in contact with the *in vitro* samples, and the fluorescent signal from the bacteria was collected with the fiber bundle and imaged onto the CCD. This information was used to characterize the sensitivity for fluorescent bacteria. Although individual bacteria would not be resolved by the imaging system, the ability to resolve bacterial colonies may indicate sufficient resolution to image regions of bacterial infection in tissue.

2.3. In situ imaging of subcutaneous infection

All animal studies were approved by the Texas A&M Institutional Animal Care and Use Committee. In this study, four female Balb/C mice were anesthetized and subcutaneously infected with bacteria in four distinct regions. Two mice were inoculated with 10^6, 10^5, and 10^4 CFU of fluorescent bacteria expressing tdTomato, and the remaining two mice were inoculated with 10^3, 10^2, and 10^1 CFU of bacteria expressing tdTomato. Each mouse was additionally inoculated with one negative control (10^6 CFU of non-fluorescent bacteria) to differentiate the signal from autofluorescence or background signal. Each inoculation site was demarcated with a 1 cm circle on the outside surface of the skin. One day following infection, the mice were euthanized and excoriated in the infection zone. The microendoscope images the tissue directly in contact with the probe, and therefore, cannot detect the bacteria through the thickness of the skin. The skin samples were first imaged using the macroscopic imaging system (Caliper LifeSciences IVIS Spectrum) to enable a later comparison with the microendoscope system. *In situ* microendoscopic imaging was performed by placing the probe in contact with the underside of the skin (Fig. 2). For each demarcated inoculation site, 20 images were taken randomly in the 1 cm region using a 100 msec camera exposure and gain setting of 6 for all sites. Samples from the prepared inocula were transferred to agar plates and incubated for a period of one month to determine the number of bacteria present by CFU using visual counting.

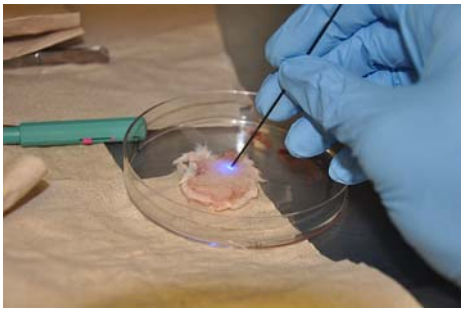

Fig. 2. Imaging of excoriated skin using the microendoscope.

#142906 - $15.00 USD Received 23 Feb 2011; revised 2 Apr 2011; accepted 4 Apr 2011; published 7 Apr 2011

2.4. In situ imaging of intra-tracheally infected lungs

Eight mice were infected intra-tracheally with bacteria (four mice common to the subcutaneous experiments). A catheter was inserted into the trachea of the anesthetized mice to administer a bolus containing 10^8, 10^7, or 10^6 CFU of fluorescent bacteria or 10^6 CFU of a non-fluorescent control, with two mice per inoculum dose. One day following inoculation, the mice were euthanized, and the lungs were removed. The lungs were first imaged using the macroscopic imaging system. With the current device, *in vivo* imaging is not possible due to the outer diameter of the fiber bundle and the lack of image guidance. The lungs were therefore cut open laterally, exposing the inner sections of the trachea and the lobes. The microendoscope probe was placed in contact with the inside surface of the tissue in ten random sites each in the trachea and lobes, in order to sample the entire area of the lungs. A 100 msec camera exposure and gain level setting of 6 were used for all sites. However, due to the high concentration of bacteria in the 10^8 CFU inoculated lungs, any images that had potential pixel saturation were also acquired with a 50 msec exposure and gain of 6. For images acquired at half the exposure time, the corresponding average intensity over the field of view was doubled for the quantification study. This was done to facilitate proper quantification of these images. Punch biopsies from lung samples were then taken using a 1mm diameter Miltex biopsy punch for imaging with a confocal microscope.

2.5. Confocal microscopy of in vitro bacterial samples and punch biopsies of intra-tracheally infected lung tissue

Smear samples of tdTomato expressing bacteria grown on agar were taken on a microscope slide for high resolution imaging on a confocal microscope. For the negative control, non-fluorescent BCG bacteria were imaged. The punch biopsies from the lung samples were fixed with 4% paraformaldehyde for 24 hours. The biopsy samples were then washed with 1 × phosphate buffer solution (PBS) twice and then transferred to a 30% sucrose solution until the samples sank down in the solution. Lung tissue was then placed on cryomold, overlaid with optimal cutting temperature (OCT) embedding media, and frozen on dry ice. Following cryosectioning of the frozen tissue, the sections were then placed on slides and stained with the nucleic acid dye DAPI. After washing with PBS, the slides were dried and mounted for viewing by confocal fluorescent microscopy.

High resolution imaging was performed on the *in vitro* bacterial smear and lung punch biopsy samples with an Olympus IX81 confocal fluorescent microscope using the DAPI, TRITC, and phase channels with exposure times of 10, 50, and 400 msec, respectively, at a 40 × magnification.

2.6. Image processing and analysis

Matlab software was used to quantify signal intensity in the microendoscope's field of view. The sub-routine averaged the pixel intensity values in the fiber bundle's active imaging area to give an average fluorescence signal for each raw image. The average and standard deviation were calculated for each inoculum. A statistical analysis using a Student's t-test was performed on the data acquired for each inoculum's signal data set ($n = 40$, subcutaneous; $n = 20$, lung) in comparison to the negative control data. The smallest inoculum whose averaged fluorescence signal was statistically higher than the negative control was taken as the system's detection limit.

Due to the heterogeneity in the bacterial distribution in tissue and the random placement of the microendoscope within the region of infection, statistically negative images were removed from the data set to evaluate correlation of average signal with bacteria. The average signal values from each image that were less than one standard deviation from the mean of the negative control were removed for the correlation analysis. The signal values from the remaining positive sites were averaged for each inoculum and plotted as a function of inoculum CFU (obtained from the plated inoculum titer). A regression fit was performed on the data to evaluate the correlation between the average fluorescence signal for each inoculum

#142906 - $15.00 USD Received 23 Feb 2011; revised 2 Apr 2011; accepted 4 Apr 2011; published 7 Apr 2011

and the CFU levels. Vertical error bars were determined by computing the standard errors using the data points remaining for each inoculum. Horizontal error bars were determined by computing the standard errors of the CFU counts for each agar-plated inoculum titer after a three week incubation period. For the lung experiments, only one set of plated inoculum titers were assessed for CFU; therefore, horizontal error bars are not included for fluorescent bacteria in Fig. 9(b) below. Since the same negative control was used in the skin and lung experiments, a triplicate inoculum titer was available for CFU measurement. As a result, an appropriate horizontal error bar for the negative control is included in Fig. 9(b).

To improve visualization of fluorescent signal in microendoscopic images of bacteria in tissue, the contrast and brightness were enhanced using ImageJ software. The dynamic range of the 8-bit images (256 gray scales) for the higher inoculum skin samples (Fig. 4) were rescaled to 0 to 200 gray scales, the lower inoculum skin images (Fig. 5) were rescaled to 0 to 60, and the lung images (Fig. 7) were adjusted to 0 to 50 gray scales. Therefore, the images within a single figure have been equally adjusted for comparison. Although this enhancement can saturate some pixels in the images of high concentration bacteria, the spatial localization of bacteria is not affected. Moreover, quantification is not affected by image enhancement, since it is performed on the raw data.

3. Results and Discussion

3.1. In vitro imaging of bacterial colonies

To assess the sensitivity of the system to image fluorescent bacteria, colonies of bacteria expressing tdTomato were imaged *in vitro*. Figure 3(a) shows an image of bacteria expressing tdTomato. Based on the signal and resolution, the image indicates that bacterial colonies expressing tdTomato can be detected and resolved well *in vitro*. Fluorescent protein colonies display strong fluorescent signal in comparison to the control that carries vector alone [Fig. 3(b)]. Based on these results, tdTomato was used as the fluorescent protein expressed by bacteria for subcutaneous and intra-tracheal infection experiments.

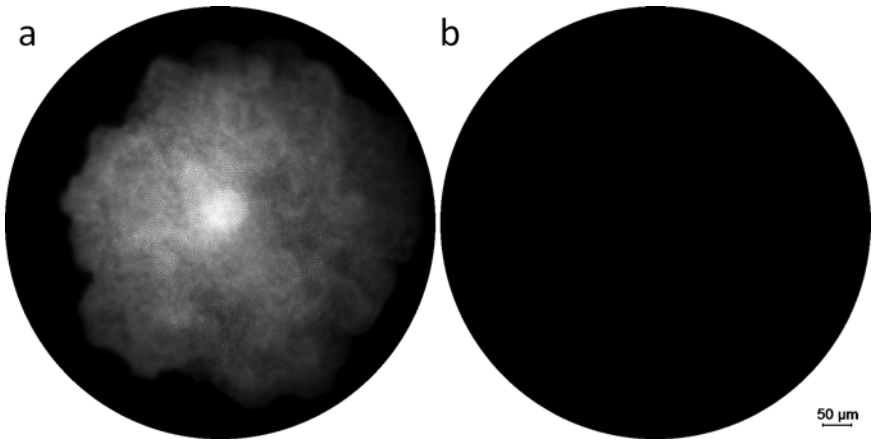

Fig. 3. Bacterial colonies grown on agar (a) expressing tdTomato, and (b) negative control (BCG carrying the vector backbone).

3.2. In situ imaging of subcutaneous infection

Imaging bacteria subcutaneously inoculated beneath the skin of mice provides controlled conditions and ease of access for characterizing the sensitivity of this system in mammalian tissue. Subcutaneously inoculated fluorescent bacteria expressing tdTomato at concentrations ranging from 10^6 to 10^1 CFU were imaged *in situ*. An image demonstrating greater than average signal within the 10^6 CFU inoculated region is shown in Fig. 4(a). Representative

#142906 - $15.00 USD Received 23 Feb 2011; revised 2 Apr 2011; accepted 4 Apr 2011; published 7 Apr 2011

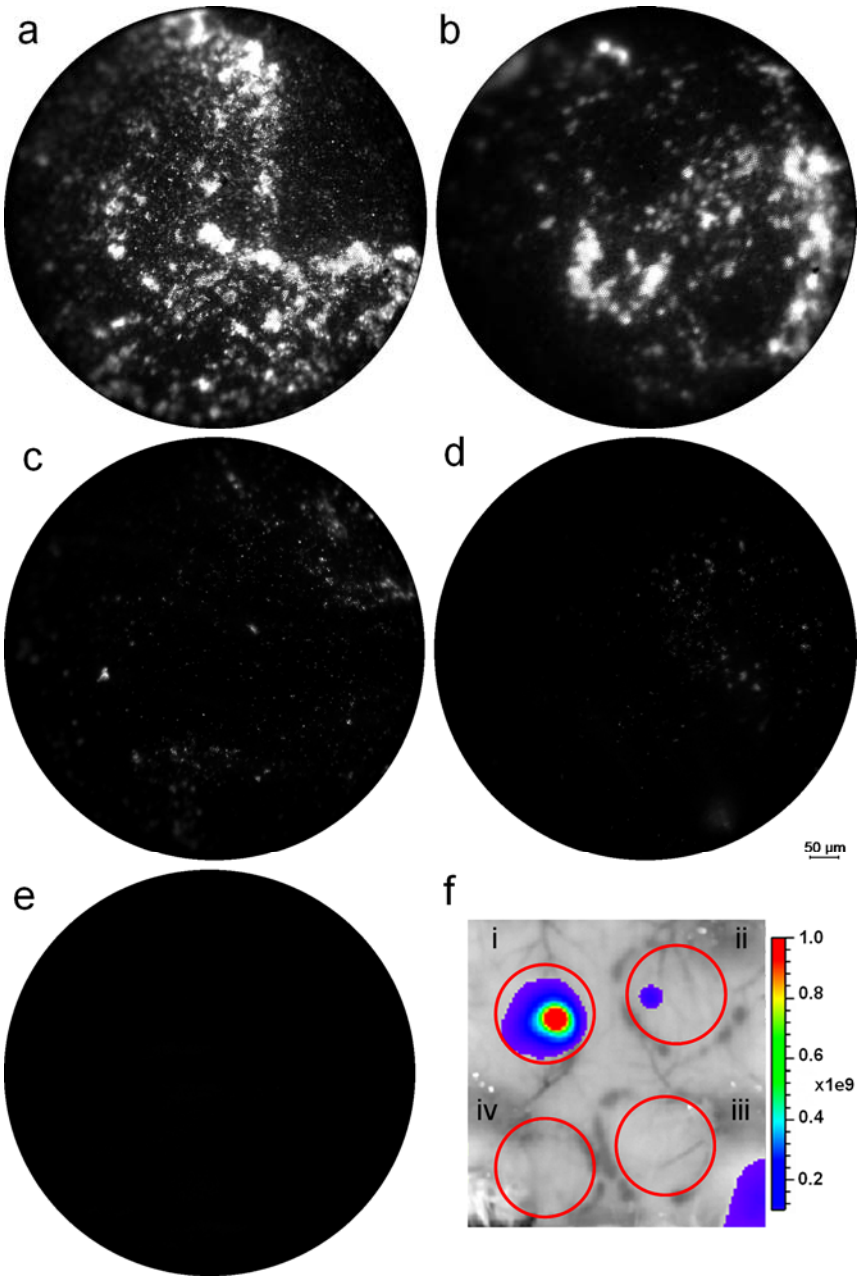

Fig. 4. *In situ* images of sites subcutaneously inoculated with (a) and (b) 10^6, (c) 10^5, and (d) 10^4 CFU of bacteria expressing tdTomato, and (e) 10^6 CFU of negative control (BCG with vector backbone). (f) Macroscopic IVIS image of tissue subcutaneously inoculated with (i) 10^6, (ii) 10^5, and (iii) 10^4 CFU of bacteria expressing tdTomato, and (iv) 10^6 CFU of negative control (BCG with vector backbone). IVIS image field of view is 6.5 cm and scale bar units are (photons/sec/cm^2/sr)/(µW/cm^2).

images of 10^6, 10^5, and 10^4 CFU sites, with average fluorescence signal within one standard deviation of the mean fluorescence for each inoculum, are shown in Figs. 4(b-d), respectively. Similarly, a representative image of the negative control is shown in Fig. 4(e). The corresponding macroscopic image taken with the IVIS Spectrum is shown in Fig. 4(f).

#142906 - $15.00 USD Received 23 Feb 2011; revised 2 Apr 2011; accepted 4 Apr 2011; published 7 Apr 2011

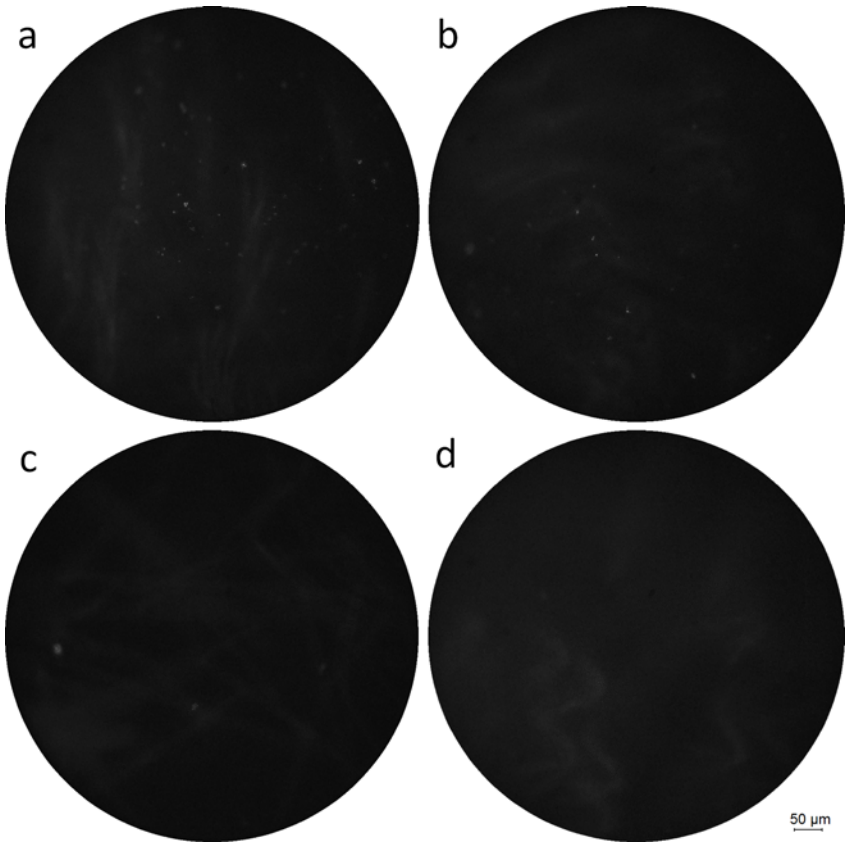

Fig. 5. *In situ* images of sites subcutaneously inoculated with (a) 10^3, (b) 10^2, and (c) 10^1 CFU of bacteria expressing tdTomato, and (d) 10^6 CFU of negative control (BCG with vector backbone).

Similarly, representative images of 10^3, 10^2, and 10^1 CFU sites are shown in Figs. 5(a-c), respectively, and an image of the negative control is shown in Fig. 5(d). Bacterial infection foci are visible at concentrations of fluorescent bacteria from 10^6 to 10^4 CFU; whereas, the negative control displays only background autofluorescence. These images are consistent with data from the macroscopic system image [Fig. 4(f)]. Tissues that had been inoculated with less than 10^5 CFU did not have visible signal when imaged with the IVIS system. For bacterial concentrations lower than 10^4 CFU, infection foci appear to be visible down to 10^2 CFU in microendoscopic images; however it is unclear whether the fluorescence is from bacteria or auto-fluorescence, especially at low inocula.

Due to the heterogeneous distribution of bacteria within the region of inoculation, there is significant variability in signal intensity depending on where the 750 µm field of view imaging probe is placed. This is demonstrated by the variation in intensity between Figs. 4(a) and 4(b), two imaging sites in the region of 10^6 CFU subcutaneous infection. In addition, there are imaging locations in close proximity to the site of inoculation that have no detectable bacterial signal. In order to average out this variability, 20 images were acquired randomly for each 1 cm region surrounding an inoculation site. It is also important to note that the actual number of bacteria detected within the fiber bundle's field of view is significantly less than the actual inoculum, since the probe's field of view is much smaller than the region of inoculation and infection.

To assess the increase in fluorescence signal with increasing inoculum dose and variation within the signal intensities of each individual inoculum, the fluorescence intensity of each image obtained for the skin samples were averaged over the field of view. The mean of the

#142906 - $15.00 USD Received 23 Feb 2011; revised 2 Apr 2011; accepted 4 Apr 2011; published 7 Apr 2011

average fluorescence signals for all images in each inoculum is plotted in a bar graph in Fig. 6(a). After removal of samples that did not have statistically significant signal, the mean fluorescence intensity was plotted versus CFU for each inoculum in Fig. 6(b).

An increasing trend is seen in the average fluorescence intensity with increasing inocula levels. A Student's t-test reveals 10^4 CFU to be the lowest inoculum with a statistically significant mean as compared to the negative control (p-value = 0.0176) as shown with a single asterisk in Fig. 6(a). The 10^5 and 10^6 CFU show much lower p-values (0.005 and 0.0004, respectively) as compared to the negative control. According to the statistical analysis, we do not find a significant signal for inocula lower than 10^4 CFU; however, what appear to be a small number of bacteria in the field of view for lower inocula can be visualized. It is possible that signal from bacteria at these lower concentrations is masked by tissue autofluorescence. Therefore, this system may be able to qualitatively detect regions of infection for 10^3 and 10^2 CFU, but quantitative assessment using our current image analysis is only possible at higher inocula. Consequently, our limit of detection of subcutaneous infection of fluorescent bacteria using this microendoscope is 10^4 CFU, in comparison to a detection limit of 10^5 CFU for the same sample using the IVIS.

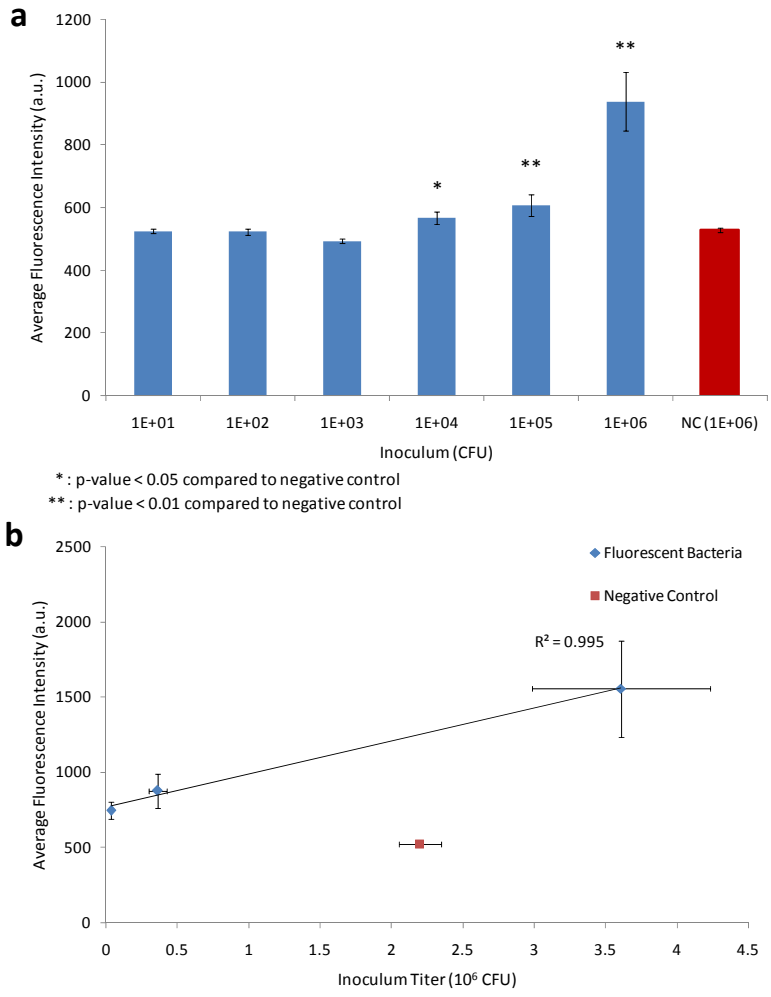

Fig. 6. Subcutaneous infection. (a) Bar plot of average fluorescence intensity for each subcutaneous bacterial inoculum. (b) Regression fit for average fluorescence intensity versus CFU levels determined from bacterial inoculum titer.

#142906 - $15.00 USD Received 23 Feb 2011; revised 2 Apr 2011; accepted 4 Apr 2011; published 7 Apr 2011

Variation in fluorescence signal increases with increasing inoculum, as indicated by the increasing size of the error bars in Fig. 6(a). This variation is visible in different imaging sites from the same inoculum dose that display varying sizes of tissue infection foci, as is seen in Fig. 4(a) and 4(b). Due to heterogeneity in the local distribution of bacteria and the small field of view, variation in numbers of bacteria within the imaging area are expected, but it should be possible to control for this variation by sampling more tissue sites.

A linear regression fit to the average fluorescence values from positive imaging sites for each inoculum versus CFU levels obtained from the inocula titer [Fig. 6(b)] has an increasing trend with an R^2 value of 0.9953 and a slope p-value of 0.0434. The regression line has a slope of 0.00022 ± 0.00012. There is a linear relationship between the average fluorescence intensities for each inoculum and bacterial CFU. These observations indicate that this imaging system may be capable of measuring bacterial numbers directly in mammalian tissues.

3.3. In situ imaging of intra-tracheally infected lungs

The lungs of the mice inoculated with BCG at various concentrations were excised and imaged with the microendoscope system. Representative images for 10^8, 10^7, and 10^6 CFU sites, with an average fluorescence signal within one standard deviation of the mean fluorescence, are shown in Figs. 7(a-c). A representative image of the negative control is shown in Fig. 7(d). These images demonstrate that regions of fluorescent bacterial infection can be detected in the lung tissue. An increasing trend in fluorescence intensity is visible in

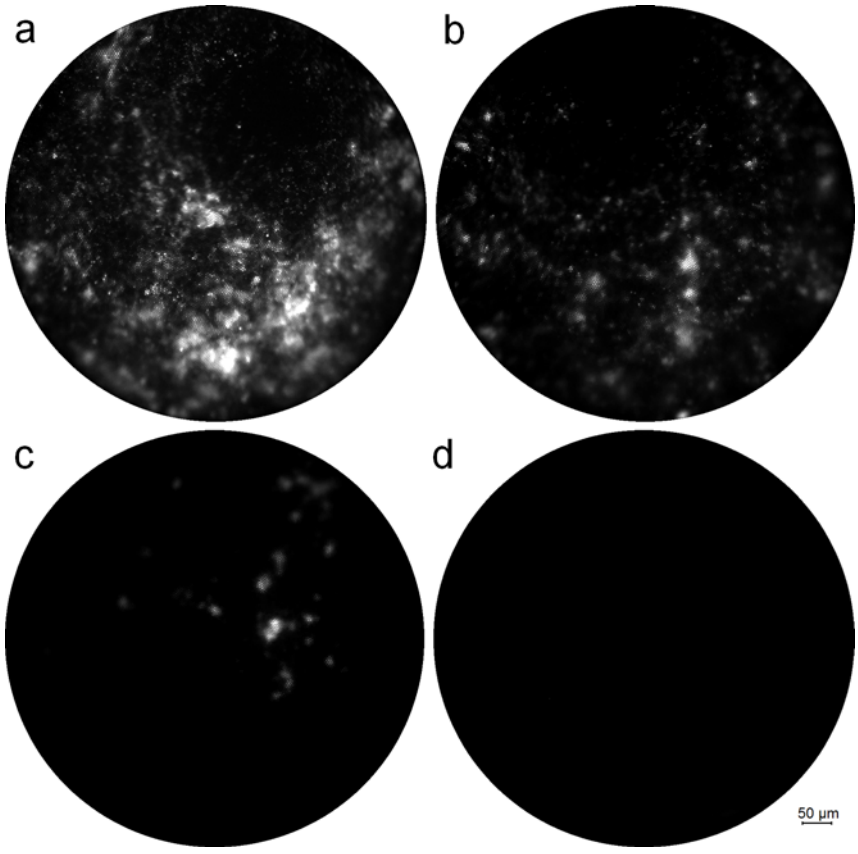

Fig. 7. *In situ* images of lungs intra-tracheally inoculated with (a) 10^8, (b) 10^7, and (c) 10^6 CFU of bacteria expressing tdTomato, and (d) 10^6 CFU of bacteria carrying vector alone (negative control).

#142906 - $15.00 USD Received 23 Feb 2011; revised 2 Apr 2011; accepted 4 Apr 2011; published 7 Apr 2011

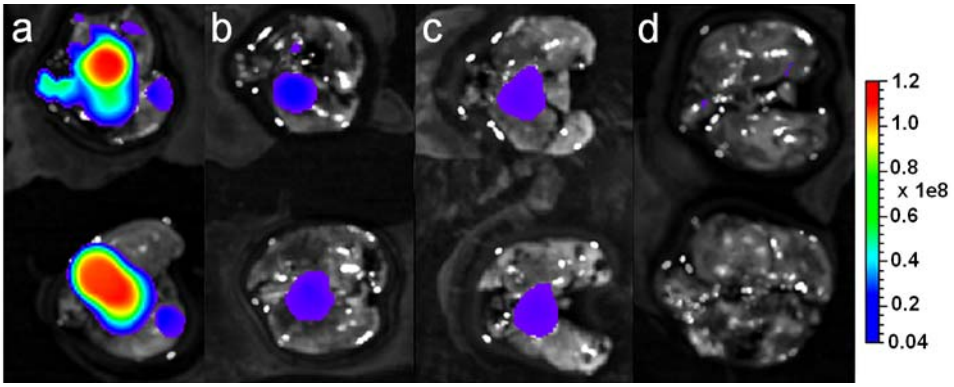

Fig. 8. Macroscopic IVIS images of lungs intra-tracheally inoculated with (a) 10^8, (b) 10^7, and (c) 10^6 CFU of bacteria expressing tdTomato, and (d) 10^6 CFU of non-fluorescent vector backbone (negative control). Field of view is 6.5 cm and scale bar units are (photons/sec/cm^2/sr)/(μW/cm^2).

the images with inocula ranging from 10^6 to 10^8 CFU. The corresponding macroscopic fluorescence images are shown in Fig. 8. Bifurcation points in the trachea are seen to have high levels of fluorescent bacteria, but bacteria are also more homogeneously distributed in deeper regions within the lobes of the lung

The average fluorescence intensity for each intra-tracheal dose is plotted in Fig. 9(a). An inoculum of 10^7 CFU produced a statistically significant signal in the lung (p-value = 0.0048) as compared to the negative control. The higher detection limit for bacteria in the lungs is most likely due to the greater distribution of bacteria in the lung in comparison to a more localized subcutaneous inoculation. Following an intra-tracheal inoculation, bacteria are distributed throughout the lung tissue, making localization difficult and offering an important potential application for microendoscopic systems.

Prior to performing a correlation analysis, images within one standard deviation of the average intensity of the negative control were removed from the data set for each inocula. Although the average signal of all the images acquired from the 10^6 CFU inoculum site was not found to be statistically significant, removal of negative images resulted in analysis of images with statistically significant signal compared to the negative control (p-value = 0.0026). The regression fit was performed for data between 10^6 and 10^8 CFU. An increasing trend in average fluorescence signal of positive sites for each inoculum versus CFU levels is seen in lung tissue [Fig. 9(b)]. The regression fit with an R^2 value of 0.9998 and a slope p-value of 0.0094 indicate a linear relationship between the average signal for each inoculum and CFU levels. The slope of the regression line has a value of 0.0000061 ± 0.0000017. These results demonstrate potential for use of this system to image and measure bacterial numbers during pulmonary infection for intra-tracheal inocula down to 10^6 CFU. Improvements in quantification of signal and quantification of bacteria in small tissue samples may enable measurement of bacterial numbers in individual images.

3.4. Confocal microscopy of in vitro bacterial samples and punch biopsies of intra-tracheally infected lung tissue

Imaging *in vitro* bacterial smear samples and sections from punch biopsies of infected lung tissue was performed with a confocal microscope to provide a high resolution image reference. *In vitro* samples of tdTomato expressing bacteria were prepared by smearing bacteria on glass slides and imaging with a confocal microscope. The results in Fig. 10(a) show both isolated and clumps of fluorescent bacteria, 4-6 μm in length, in the TRITC (red) channel, while no fluorescence was observed for the negative control in Fig. 10(b).

#142906 - $15.00 USD Received 23 Feb 2011; revised 2 Apr 2011; accepted 4 Apr 2011; published 7 Apr 2011

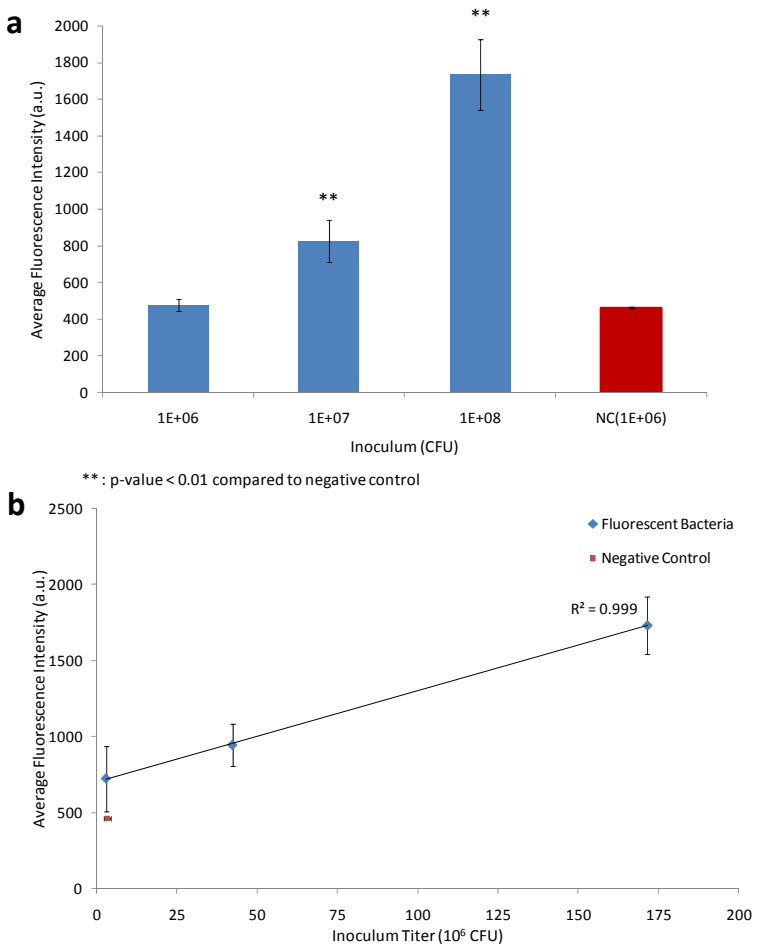

Fig. 9. Lung infection. (a) Bar plot of average fluorescence intensity for each intra-tracheal (lung) bacterial inoculum. (b) Regression fit for average fluorescence intensity versus CFU determined from bacterial inoculum titer.

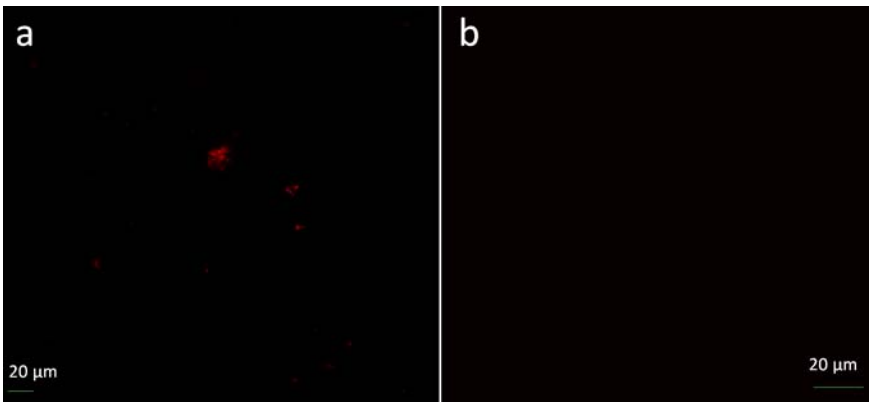

Fig. 10. Confocal microscope images of *in vitro* smear samples prepared using (a) tdTomato expressing BCG bacteria and (b) non-fluorescent BCG bacteria

#142906 - $15.00 USD Received 23 Feb 2011; revised 2 Apr 2011; accepted 4 Apr 2011; published 7 Apr 2011

Confocal images of sections of infected lung punch biopsies are shown in Figs. 11(a)-(f). The nuclei of cells in lung tissue were counter stained with DAPI for ease of visualization. Images of tdTomato expressing bacteria in the TRITC and DAPI + TRITC channels in Figs. 11(b) and 11(c) reveal fluorescent bacteria lodged within tissue. Bacterial fluorescence is absent in the TRITC and DAPI + TRITC channels for images of the non-fluorescent negative control in Figs. 11(d)-(f).

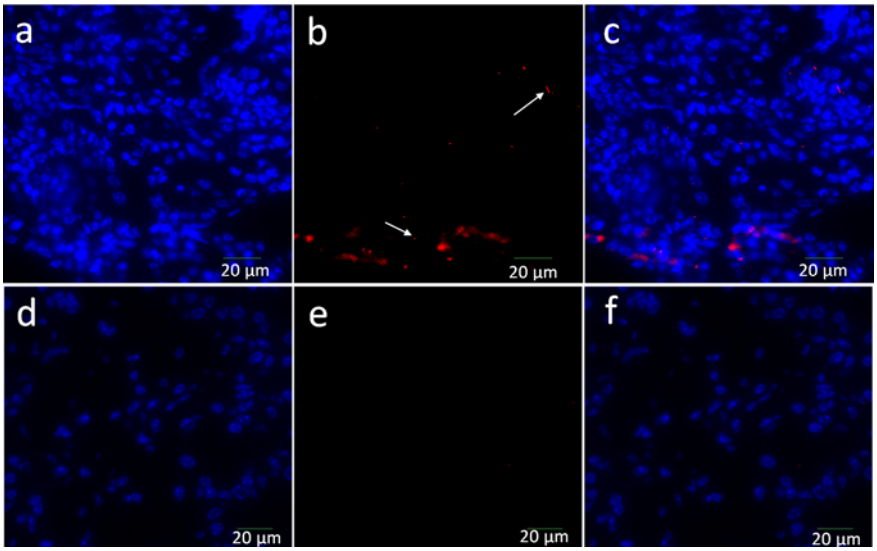

Fig. 11. Confocal microscope images of histology slides prepared using punch biopsies of lung tissue infected with (a), (b), and (c): tdTomato expressing bacteria; (d), (e), and (f): non-fluorescent BCG bacteria. (a) and (d): DAPI (blue) channel; (b) and (e): TRITC (red) channel; (c) and (f): DAPI + TRITC channels. White arrows indicate tdTomato expressing BCG bacteria.

4. Conclusion

We have constructed a fluorescence microendoscope with a resolution of 4 µm and a 750 µm diameter field-of-view. *In vitro* imaging of bacteria expressing tdTomato demonstrated the system's capability to detect and resolve bacterial colonies. *In situ* imaging of mice subcutaneously and intra-tracheally infected with bacteria expressing tdTomato confirmed similar imaging capability at the tissue level. Well resolved regions of bacterial infection were visible for subcutaneous inocula of 10^6 to 10^4 CFU and intra-tracheal inocula of 10^8 to 10^6 CFU. The average fluorescence signal from bacteria in the skin and lung images have a linear relationship with CFU, suggesting the potential of this system to obtain quantitative data. This is confirmed with the increasing trend seen in the bar plots for the average fluorescence versus inoculum dose as well as the linear trends for the average fluorescence versus CFU from inoculum titer.

Based on statistical analysis of the quantified images, the microendoscope's limit of detection was determined to be 10^4 CFU in the case of skin samples and 10^7 CFU for lung samples. It is possible that bacteria can be detected qualitatively at inocula down to 10^2 CFU in skin, but bacterial detection may be confused with anatomical features that contribute to autofluorescence. Additionally, bacteria were qualitatively visible in lungs intra-tracheally infected with 10^6 CFU of fluorescent bacteria, which was the lowest inoculum tested in this experiment. Improvements in image analysis may lower the level of detection.

Images of *in situ* lung tissue infected with fluorescent bacteria display regions of significant fluorescence as compared to that infected with non-fluorescent bacteria. In addition, there is a linear relationship between the average fluorescence for each inoculum and the CFU inoculated. High resolution confocal images of punch biopsies from infected lung

#142906 - $15.00 USD Received 23 Feb 2011; revised 2 Apr 2011; accepted 4 Apr 2011; published 7 Apr 2011

tissue also confirm the presence of fluorescent bacteria embedded in lung tissue. The microendoscope's *in situ* imaging results provide proof of concept and suggest that this device shows promise for *in vivo* imaging using a smaller fiber bundle that can be delivered directly into the lungs via a catheter. Initially, *in vivo* imaging of higher inoculation doses may be guided by whole body fluorescence imaging scanners. Subsequently, imaging of infection of bacterial concentrations below the detection limit of the whole body scanners may be possible. Another potential application for this microendoscope is the imaging and detection of bacteria in bronchial washings, which are typically analyzed via microscopic analysis for the diagnosis of pulmonary tuberculosis infections [25,26]. Since our system relies on fluorescence from the genetically-modified bacteria for detection and bacteria extracted from bronchial washings are non-fluorescent, bacteria may be detected via fluorescent reporters. One possible method is the use of fluorogenic substrate probes to detect endogenous β-lactamase enzyme, which is naturally expressed by *Mycobacterium tuberculosis*, in a reporter enzyme fluorescence scheme [27].

Use of a microendoscope may provide the capability to image fluorescent bacteria directly within its host environment to better understand disease progression. Modification of the system for dual channel imaging of cells expressing GFP and bacteria expressing tdTomato may enable detailed investigation of cells that phagocytose bacteria and their dynamics *in vivo*. This may aid in visualizing and gaining insight into how bacteria at low inocula concentrations from the lungs, the site of initial infection by tuberculosis, spread into extra-pulmonary regions, the details of which are currently not well understood.

Acknowledgments

This work was supported in part by the Bill and Melinda Gates Foundation grant no. 48523. We also thank Ms. Rachel Schaffer for her initial work on the project.

#142906 - $15.00 USD Received 23 Feb 2011; revised 2 Apr 2011; accepted 4 Apr 2011; published 7 Apr 2011